Comparison of Dual Water Vapor Radiometer Differenced Path Delay Fluctuations and Site Test Interferometer Phase Delay Fluctuations Over a Shared 250-Meter Baseline

David D. Morabito,* Larry R. D'Addario,† Stephen Keihm,‡ and Shervin Shambayati▲

ABSTRACT. — Site test interferometers (STIs) have been deployed at Goldstone, California, in order to (1) assess the suitability of Goldstone as an uplink array site, and (2) statistically characterize atmospheric-induced phase fluctuations over a ~250-m baseline for the Goldstone climate for use in future array link scenarios. Beginning in August 2008, dual water vapor radiometers (DWVRs) were deployed next to each antenna element of the STI residing at the Venus site at Goldstone forming a baseline of similar length. The differenced path delay between the two WVR units forms an additional data type that can be used to validate the STI phase fluctuations and confirm the atmospheric nature of these fluctuations. This study was motivated by several considerations. First, the use of a single WVR provides single-point path delay fluctuation measurements that could be used as an ancillary data type, to compare against the magnitude of STI path delay fluctuations. Second, the use of two WVRs allows estimation of their differenced path delay, which produces a data type that could be correlated directly against the STI phase difference fluctuations (filtered to remove long-period nontroposphere variations). This can allow one to assess whether STI fluctuations are due to troposphere or can be used to identify suspicious signatures to verify whether equipment problems or other anomalies exist. Such an experiment could also be used to explore the feasibility and limitations of using a DWVR in place of an STI to characterize atmospheric phase fluctuations for a generally "dry" climate when liquid content in the atmosphere is minimal (up to a certain limit occurring less than 1 percent of the time). This article reports on initial study results of a comparison of differenced path delay statistics derived from both the DWVR and the STI, as well as including discussion of prospects for future DWVR experiments using WVRs of improved design and optimal experimental procedures.

* Communications Architectures and Research Section.
† Tracking Systems and Applications Section.
‡ Instrument Systems Instrumentation and Concepts Section.
▲ Space Systems Loral, Communications Systems Department.

The research described in this publication was carried out by the Jet Propulsion Laboratory, California Institute of Technology, under a contract with the National Aeronautics and Space Administration.

I. Introduction

Water vapor radiometer (WVR) data have been used to calibrate or experimentally characterize atmospheric error sources in phase data gathered from radio science experiments [1] and very long baseline interferometry (VLBI) experiments [2]. Simultaneous VLBI and WVR experimental measurements on a 21-km baseline within the Deep Space Network's (DSN's) Goldstone, California, tracking site demonstrated that WVRs removed a sizable contribution of tropospheric delay fluctuations from the VLBI data type [2]. A good review article on the extraction of path delay from microwave radiometry can be found in [3].

A site test interferometer (STI) has been deployed at the Venus Deep Space Station–13 (DSS-13) antenna site at Goldstone, California, in order to assess Goldstone as an uplink array site, and statistically characterize atmospheric-induced phase fluctuations over a 250-m baseline for use in future array link scenarios. These statistics can be used in the estimation of array loss for given array configurations by appropriate scaling of the STI elevation angle, STI frequency, STI altitude above mean sea level, and STI element spacing to those of the array [4–6].

The STI located at the Venus Goldstone site is composed of two 1.2-m-diameter antennas (and associated equipment) separated by ~250 m in a generally east–west configuration at the Goldstone Venus site pointed at the geostationary ANIK F2 broadcast satellite at an elevation angle of 48 deg. The 20.2-GHz carrier tone emitted by ANIK F2 is the signal source. The first year of STI statistics has been estimated from data acquired from May 2007 to April 2008. The first year's results are documented in a series of papers published elsewhere [6–8]. Since then, several additional years of data have been acquired.

WVRs are instruments that measure sky brightness temperature at selected frequencies around the 22-GHz water absorption line. By utilizing radiosonde-derived correlations of theoretical WVR brightness temperature with integrated water vapor and cloud liquid, the WVR measurements can be interpreted in terms of wet path delay and integrated liquid water abundance [9]. The wet path delay fluctuations measured by the WVRs are dominant over those of the dry troposphere for the timescales of interest (<600 s). The use of a single WVR provides single-point path delay fluctuation measurements at the site that could be used as an ancillary data type in which to correlate against path delay variations measured across an STI baseline. By placing WVRs next to each element of an STI baseline, one can make a reasonably "equivalent" system where the measured path delays from each WVR unit can be differenced and filtered, and the result compared to the STI phase estimates (after longer-term satellite motion and instrumental drift have been filtered out). This system is defined herein as a dual water vapor radiometer (DWVR) instrument in which the differenced path delay is the observable of interest. Beginning in August 2008, two WVR units were deployed next to each element of the Goldstone Venus STI in an attempt to provide a means of validation of the STI phase fluctuations as being tropospheric in character and to also explore the feasibility and limitations of using a DWVR in place of (or complementary to) an STI to characterize atmospheric phase fluctuations for generally "dry" climate sites. The comparisons can also be used to diagnose suspicious signatures in the STI data for the purposes of identifying potential problems or anomalies. DWVR data can also be used to

provide statistics in place of those of an STI for dry climate sites or during conditions of low atmospheric liquid content (up to a certain threshold).

Figure 1 depicts an overhead aerial photo of the Venus site at Goldstone annotated with the locations of the two STI elements and those of the two WVR instruments. Each WVR unit was placed near an STI element, also forming an approximately equivalent 250-m east–west baseline for the WVRs. The JT2 WVR was placed next to the STI element that lies next to the 34-m-diameter beam-waveguide (BWG) Research and Development (R&D) antenna (designated as DSS-13). The D1 WVR unit was placed next to the STI element residing next to the Venus site operations building. All elements were pointed at the ANIK F2 geostationary satellite (except for the small amount of time when the WVRs were performing tipping curve calibrations). The D1 and JT2 units are older model WVRs that have since been replaced by the advanced WVR (AWVR) in the operational DSN. The D1 unit operates at frequencies of 20.7 and 31.4 GHz and the JT2 unit operates at 20.7, 22.2, and 31.4 GHz. The AWVR operates at frequencies of 22.2, 23.8, and 31.4 GHz. The most important difference between the older (JT2 and D1) WVRs and the AWVR is a 2 to 3 order of magnitude difference in the thermal stability at hour timescales, resulting in an order of magnitude calibration improvement in AWVR calibration stability. The older units all could be programmed to track a source in the sky (and they were at one time), but they were limited by elevation pointing precision at the ~0.5 deg level (as opposed to the AWVR elevation pointing precision of ~0.05 deg). For this experiment, the available JT2 and D1 units remained fixed at the position of the geostationary ANIK F2 satellite in the sky except when performing calibrations. The two WVRs sampled sky brightness temperature at multiple frequencies away from the 20.2-GHz signal frequency emitted by the satellite.

This article presents initial study results of a comparison between differenced path delay statistics from an STI instrument and a DWVR instrument as well as discussion of potential error sources. This article also presents suggestions for improvements in the DWVR instrument and future experiments using improved WVRs and experimental procedures.

Figure 1. Aerial photo of Goldstone Venus site showing locations of STI elements and WVR units. (Photo credit: Dane Garvin and ITT Exelis)

II. Observations and Analysis Approach

The prime data used for the comparison were acquired during the one-month period of August 2008, which initiated the second year of data collection for the Goldstone Venus STI. We focused on the August 2008 DWVR data set to make the DWVR/STI comparison because there were fewer problems with the aging WVRs during their initial deployment that month versus later months. In addition, the largest amount (and variation) of atmospheric water vapor and the warmest temperatures were obtained during the hot summer days of August 2008, resulting in the largest amount of induced path delay fluctuations. This allowed for the best sensitivity in performing such a comparison using suboptimum and aging (but available) WVR instruments.

A. STI Data Processing and Analysis

The August 2008 STI data were first examined to identify and filter out anomalous data points. The data acquired prior to August 1, 16:33 UTC (1.69 day), were removed from the data set prior to the comparison because site maintenance activities were in progress during that time. The in-phase (I) and quadrature-phase (Q) samples of the received satellite signal from each antenna element were recorded at 1-s time resolution. The four-quadrant signal phase at each antenna was then estimated using the ATAN(Q/I) function. The signal phases between antenna elements were differenced and unwrapped (or adjusted) for cycle ambiguities, forming the differenced STI phase.

The differenced STI phase was converted to zenith path delay by dividing by the sky frequency of the satellite signal and multiplying by the sin of the elevation angle of the satellite. The resulting STI differenced path delay time series for the month of August 2008 as derived from the STI phase data shows a generally diurnal signature (see Figure 2). Figure 3 displays this variation more clearly for a selected one-day period (August 26, 2008). This diurnal variation is caused by satellite motion as it drifts from its assigned geostationary orbit position (but still lying within the beamwidth of each fixed STI antenna element). Other contributions to the variations in phase include the effect of periodic stationkeeping maneuvers on the spacecraft (performed to keep the satellite in its assigned "box" in the sky[1]), and instrumental drift caused by thermal temperature variations in the equipment such as diurnal daytime heating/nighttime cooling and component aging. The light-time latency of the satellite signal arrival between STI elements was negligible and thus no correction to the STI phase difference was necessary.

We are unable to extract tropospheric phase delay and its fluctuation energy directly from the raw STI path delay due to contributions from satellite motion and instrumental drift. Fortunately, these contributors are insignificant at the timescales where tropospheric fluctuations dominate and thus can be filtered out. Long-period trends in each 10-min block of data were thus removed using second-order polynomial fitted models. It is believed that the troposphere dominates at short timescales (order of seconds to several tens of seconds)

[1] Timothy Douglas, personal communication, Telesat Canada, July 2008.

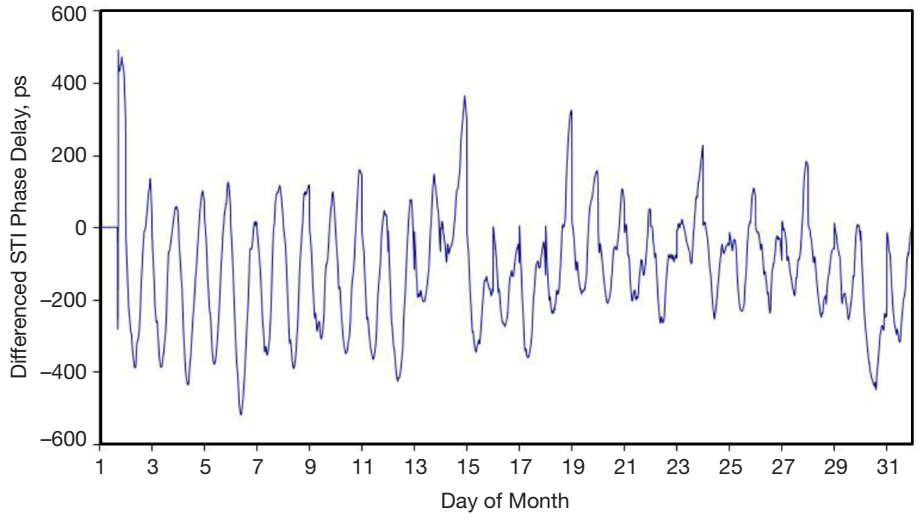

Figure 2. Differenced STI phase (or path) delay (referenced to zenith) for August 2008 showing a combination of diurnal satellite motion and instrumental drift prior to removal of second-degree polynomial fits in 1200-s blocks.

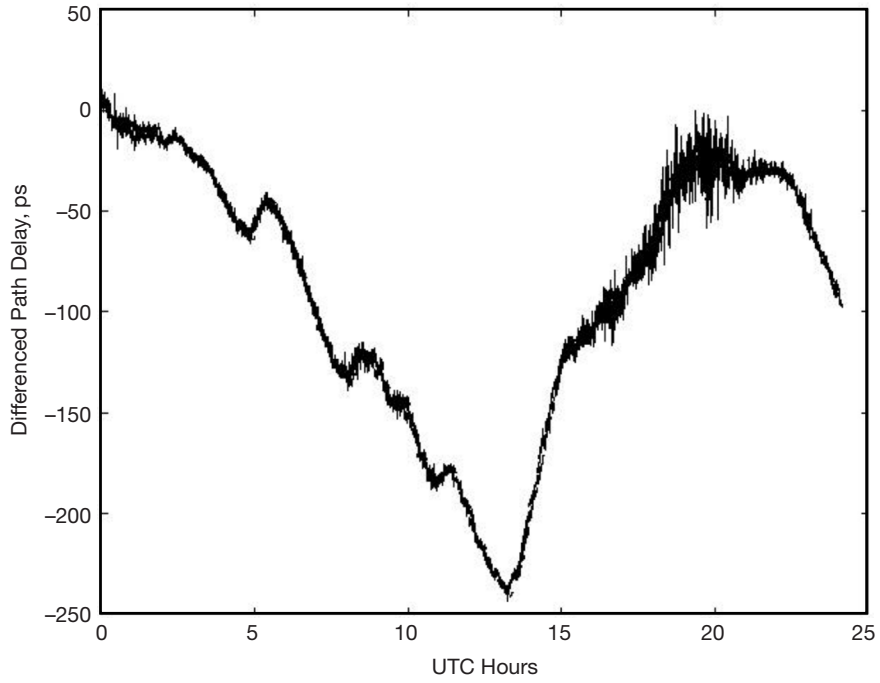

Figure 3. STI differenced phase (or path) delay (referenced to zenith) for a selected one-day period (August 26, 2008) from the data of Figure 2 prior to removal of long-period trended model.

after removing the fitted model from each 600-s block of data [7–8]. Figure 4 displays these residuals for the selected one-day period of August 26, 2008. The higher level of fluctuation occurs during the few-hour period centered about local noon (~19:00 UTC).

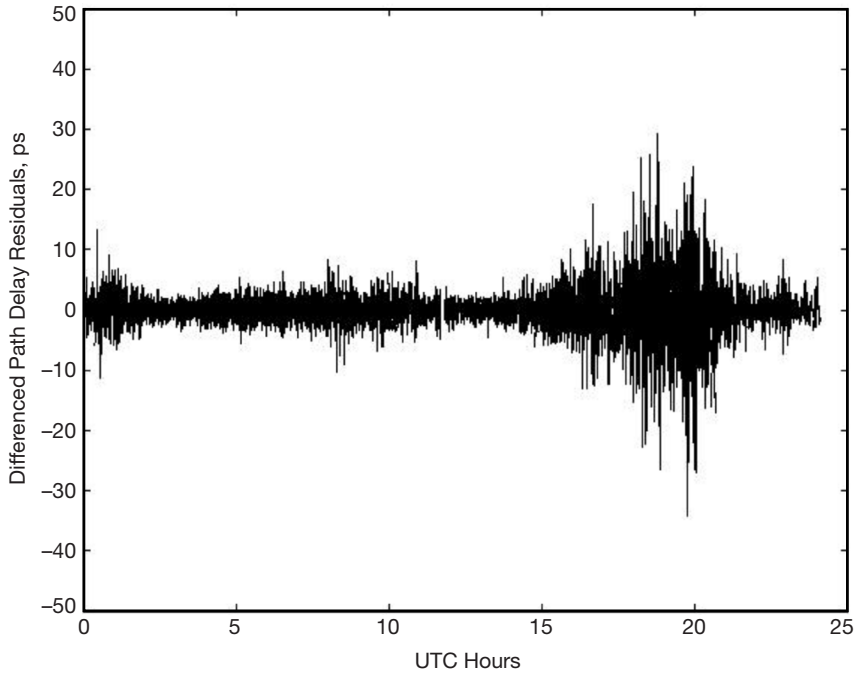

Figure 4. STI zenith path delay residuals for a selected day (August 26, 2008) from the data of Figure 2 after removal of long-period trended model.

Figure 5 displays the path delay scatter (referenced to zenith) for August 26, 2008 for 600-s blocks. Given that the use of 600-s blocks was found to be problematic for the comparison with the noisier DWVR data, it was decided to use 1200-s blocks for this study. The RMS scatter of the residual STI phase delay data (or differential path delay scatter) over each 1200-s block was thus estimated in preparation for comparison with the equivalent measure for the DWVR, resulting in 72 estimates during each one-day period. This statistical measure is meaningful in that it can be related to atmospheric decorrelation effects across spatial distances comparable to antenna array element separations and thus be converted to array loss for potential future antenna arrays [4–6].

The STI phase delay scatter is believed to include a small 0.158 ps contribution due to instrumental thermal noise, which was consistent with the levels measured during zero-baseline tests performed in Cleveland, Ohio, at NASA's Glenn Research Center (GRC) [7] and also lay close to minimum values observed during the overall yearly STI data collection [6].

B. DWVR Data Processing and Analysis

The spatially separated WVR pair (or DWVR) was co-located with the STI on a similar ~250-m east–west baseline and both instruments were pointed at the geostationary ANIK F2 satellite that emitted a 20.2-GHz beacon signal for the STI. Thus, both instruments were sampling the same general volume of sky; however, there were expected to be some differences with the STI due to beam mismatch and beam offset as well as a contribution due to the small difference in DWVR and STI baseline lengths. The beamwidths of the WVRs being wider than those of the STI antennas results in beam mismatch, one potentially significant

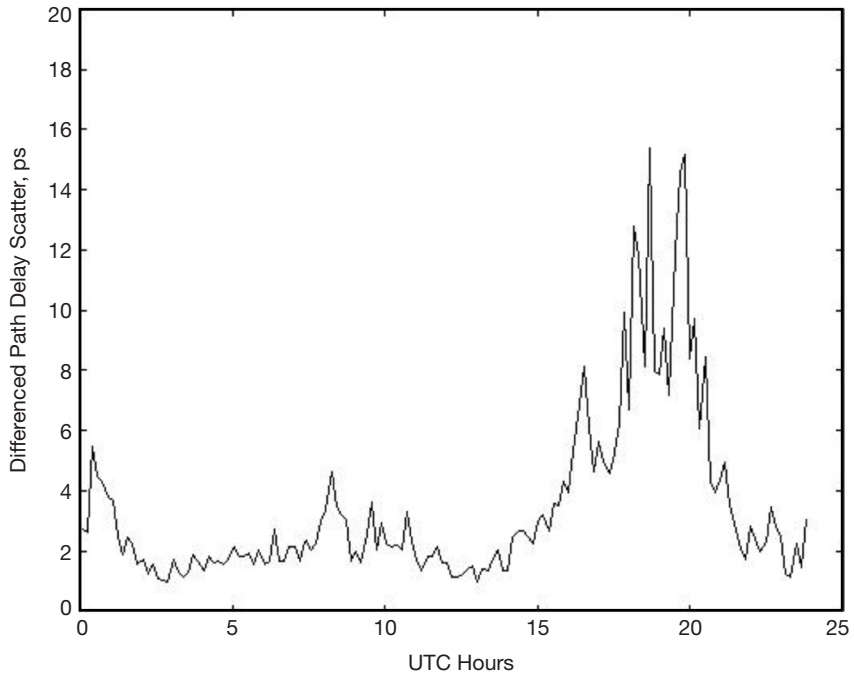

Figure 5. STI zenith delay residual scatter (ps) in 600-s bins for the selected one-day period of August 26, 2008.

error source that requires further study and quantification. Another potential significant error source is beam offset since the WVRs are located several meters away from each nearby STI element. These error sources along with others are discussed in Section IV.

The WVRs performed calibrations every ~30 min in the form of tip curves for a short period of time. These tip curve sequences were not synchronized and resulted in longer gaps, which made the differencing algorithm between the J- and D-unit WVR data points inefficient and more complicated.

The zenith path delays for each WVR were obtained from the measured sky brightness temperatures based on retrieval algorithms developed for each WVR. For the JT2 WVR unit, line-of-sight sky brightness temperature (TB_{los}) was measured at 20.7, 22.2, and 31.4 GHz at 8-s time resolution. For the D1 WVR unit, line-of-sight sky brightness temperature measurements (TB_{los}) were acquired at 20.7 and 31.4 GHz at 34-s time resolution.

TB_z represents zenith equivalent brightness temperatures derived from the line-of-sight TB_{los} measurements using an "effective radiating temperature" of the atmosphere, T_{eff}, in the following formulation:

$$TB_z = T_{eff} - (T_{eff} - T_{cos})\left[(T_{eff} - TB_{los})/(T_{eff} - T_{cos})\right]^{\sin(\theta)} \quad (1)$$

where T_{cos} = 2.73 K is the cosmic background contribution to TB and θ = 48.65 deg is the fixed elevation angle of the geostationary satellite. In general, T_{eff} is slightly dependent on frequency and surface air temperature. Without knowledge of the surface temperature, a constant value of T_{eff} = 285 K was used in Equation (1) and assumed to not significantly alter the results.

All-weather algorithms (i.e., zenith wet delay) were used to retrieve wet path delay from the brightness temperature measurements for the August 2008 WVR data sets. For the D1 unit, the wet path delay in cm is given in terms of the brightness temperatures at each frequency by

$$\Delta\rho_z = 8.13 + 0.634(\mathrm{TB}_{z,20.7} - 21.09) - 0.265(\mathrm{TB}_{z,31.4} - 15.06) \quad (2)$$

For the JT2 unit (three frequencies), the wet zenith path delay in cm is given by

$$\Delta\rho_z = 8.13 + 0.9363(\mathrm{TB}_{z,20.7} - 21.09) - 0.1643(\mathrm{TB}_{z,22.2} - 32.08) - 0.3299(\mathrm{TB}_{z,31.4} - 15.06) \quad (3)$$

The individual WVR data path delays in cm (Equations 2–3) were converted to units of ps and were then processed to produce estimates of differenced D1-unit – JT2-unit path delay. The standard deviation of this difference was estimated over 600-s (and 1200-s) intervals made to be consistent with those of the STI data intervals. Complications arose because the two WVR units had different integration and sampling times and the calibrations were being performed at different times between the two elements. Thus, a nontrivial interpolation scheme was needed. This scheme included interpolating the data across gaps that occurred during tipping curve calibrations. Three different interpolation schemes were examined, and the one that performed best (lowest scatter on path delay differences) was selected for use in the comparison.

The delivered WVR data files were time-tagged with the fractional number of days since the start of the month (i.e., 0.5 refers to 12:00 UTC of the first day of the month). The time tags were corrected to the monthly day-number by adding one to each value. The J-unit WVR path delays were interpolated to the time tags of the D-unit using a nontrivial interpolation scheme.[2] Thus, additional noise on the DWVR data was expected due to interpolating the data points taken at different sample times and across tip-curve calibration gaps.

Figure 6(a) displays the zenith path delay time series acquired from both D-unit and J-unit WVRs during August 2008. The agreement between the two data sets is reasonably good as expected. The path delay reaches values as low as 70 ps (2 to 3 cm) and above 700 ps (20 to 25 cm) during the month of August 2008. Upon close inspection of the differenced path delay between these two data sets (Figure 6[b]), we see that the difference does not exceed 80 ps (3 cm) and that there is evidence of some trends and jumps (such as near days 2.9, 20.5, and 25.9), presumably related to equipment issues. We assume that these features do not appreciably affect the overall statistics and can easily be corrected or removed from the data set. The quantity of interest extracted from these data will be its standard deviation within each 600-s (or 1200-s) block of data to then be compared with the equivalent quantity extracted from the STI data series discussed in Section II.A.

The effect of the different baseline lengths on the path delay scatter between STI and DWVR data sets can be corrected by making use of the structure function approach:

[2] S. Shambayati, "Calculating the Differences between J-Unit and D-Unit Path Delay Measurements," JPL Interoffice Memorandum 332B-09-SS02 (internal document), Jet Propulsion Laboratory, Pasadena, California, December 2009.

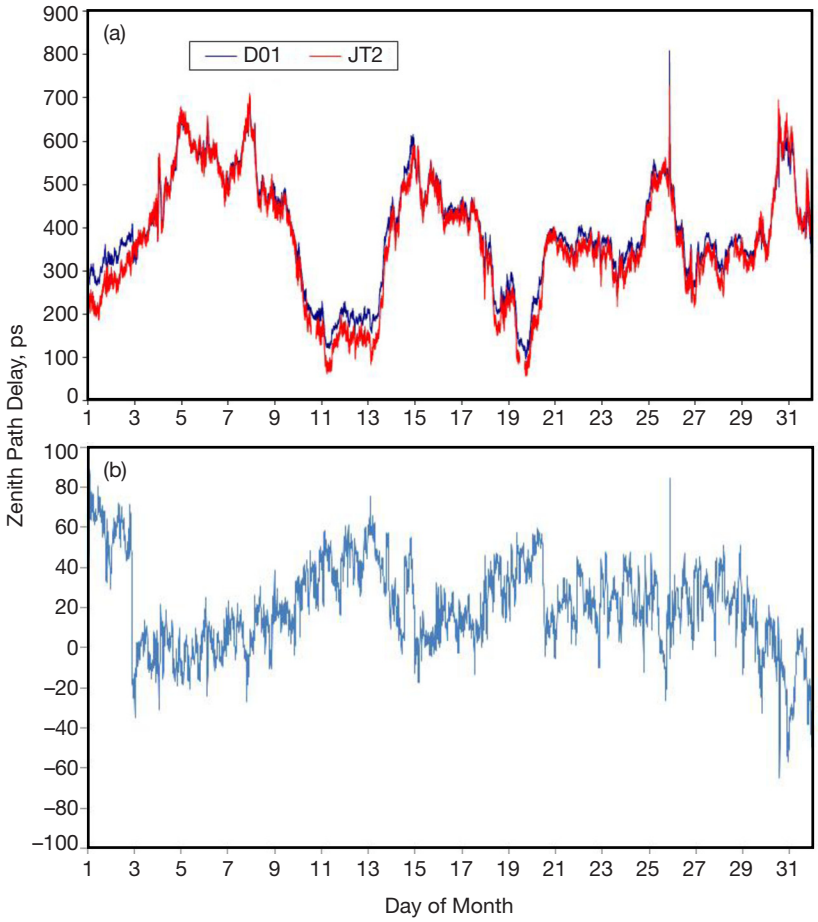

Figure 6. (a) Retrieved August 2008 zenith path delay time series for D1-unit WVR (blue) and JT2-unit WVR (red), and (b) differenced (D1-JT2) zenith path delay.

$$\sigma_{STI} = \sigma_{\mathrm{DWVR}} \left(\frac{r_{STI}}{r_{DWVR}} \right)^{\beta/2} \tag{4}$$

where r_{STI} is the length of the STI baseline and r_{DWVR} is the length of the WVR baseline.

The two baseline lengths were measured via inspection of the locations of the various instruments in the aerial photo (Figure 1) and it was determined that the ratio $r_{STI}/r_{WVR} = 0.933$. Given the hot humid summer conditions expected in August 2008, we adopted a value of $\beta = 5/3$ for the exponent in Equation (4). The resulting factor of 0.95 was then available to multiply against the DWVR scatter to allow an equitable comparison against that of the STI.

III. Results: Comparison of DWVR and STI Path Delay Fluctuations

Figure 7(a) displays the zenith differenced path delay residuals extracted from the STI processing for the selected day of August 26, 2008 (Figure 4 repeated) and Figure 7(b) displays the DWVR path delay residuals for the same day after filtering out long period (nontropo-

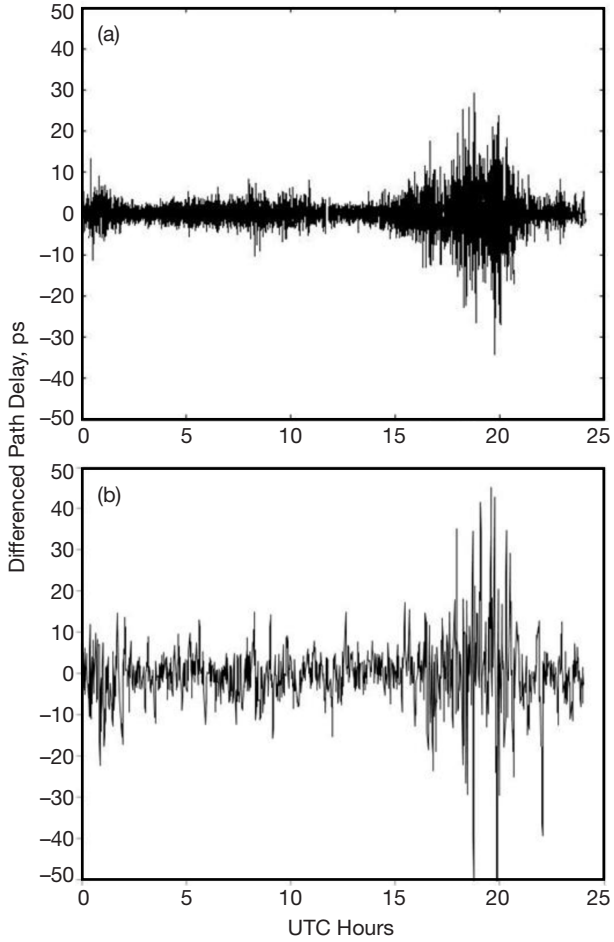

Figure 7. (a) STI differenced path delay residuals for August 26, 2008; (b) DWVR path delay residuals for August 26, 2008 (after filtering out long-period instrumental trends).

spheric) instrumental trends. As can be seen, there is apparent correlation between the two data sets where the active period, centered about local noon (~19:00 UTC), stands out in both data sets. It is noted that the DWVR series has higher scatter, but at lower temporal resolution due to the longer period sampling of the WVR data sets and the intricate interpolation algorithm applied.

Plotted in Figure 8 is the time series of standard deviation of differenced path delay (referenced to zenith) in 20-min blocks acquired from both DWVR and STI instruments over a 250-m baseline for August 2008. It appears that there are significant correlations between the STI differenced phase (or delay) fluctuations and the WVR differenced path delay fluctuations. The two time series are not identical but appear to be highly correlated and close enough in agreement to warrant further examination. The DWVR data are inherently noisier, and additional errors are incurred due to interpolating across calibration gaps and unsynchronized time tags. In addition, the WVRs are measuring the average delay among all directions within their ~6-deg-wide beams, whereas the STI is measuring the delay difference along the narrow line-of-sight path to a point-like satellite.

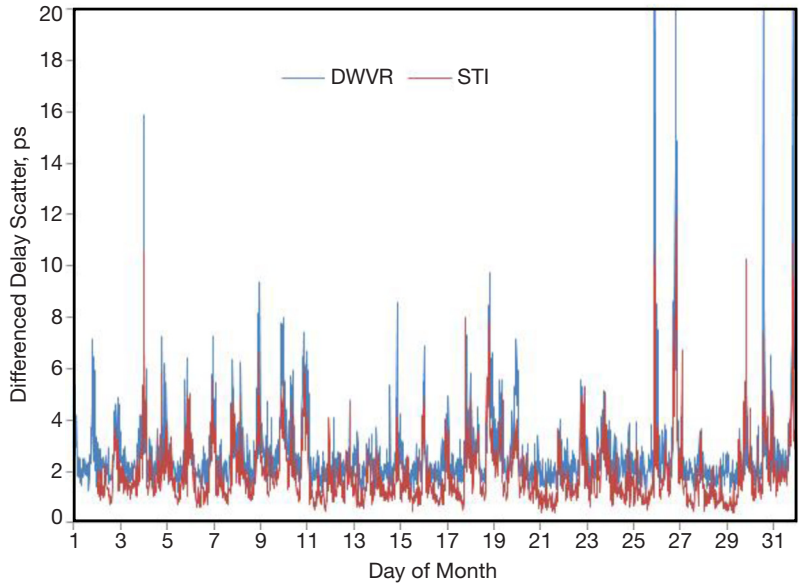

Figure 8. Goldstone Venus STI and DWVR zenith differenced path delay scatter (standard deviation in 1200-s blocks) for the month of August 2008.

In order to facilitate comparison between the differenced path delay standard deviation of the two data sets, we removed estimates of instrumental noise in a quadratic fashion from each time series: 0.158 ps of instrumental noise from the STI data and 1.3 ps of instrumental noise from the DWVR data. The DWVR noise estimate of 1.3 ps was obtained using the known WVR integration times, bandwidths, and system noise temperatures[3] as well as mapping the noise using coefficients from the chosen interpolation process.

Once we remove the noise estimates from the standard deviation estimate for both STI and DWVR, the difference in the baseline bias between the two data sets is significantly reduced, resulting in an improved agreement as visually inferred upon inspection of Figure 9.

The statistics on the path delay scatter data were examined for both DWVR and STI August 2008 data sets. The minimum STI path delay scatter was 0.268 ps, and for the DWVR it was near this arbitrary chosen threshold. The DWVR data set included several points with delay scatters that were much higher than that of the STI (although they almost always coincided with the peaks of the STI, usually during mid-day when the fluctuation in water vapor content was higher and it was warmer). The maximum path delay scatter for the STI data was 13.28 ps and for the DWVR data set it was much higher, about 41.52 ps. The higher path delay scatter for the DWVR data set may be attributed to artifacts introduced by the interpolation algorithm and beam mismatch as well as other effects. The average value of the standard deviation measurements over this one-month period was about 1.82 ps for the STI data set and about 2.83 ps for the adjusted DWVR data set. Thus, the DWVR data has ~1 ps of additional noise, due to a combination of atmospheric and nonatmospheric contributions.

[3] For the D-unit: T_{sys} of 1000 K, bandwidth of 100 MHz, and integration time of 34 s. For the J-unit: T_{sys} of 1500 K, bandwidth of 160 MHz, and integration time of 8 s. Alan Tanner, personal communication, Instrument Systems Implementation and Concepts Section, December 2008.

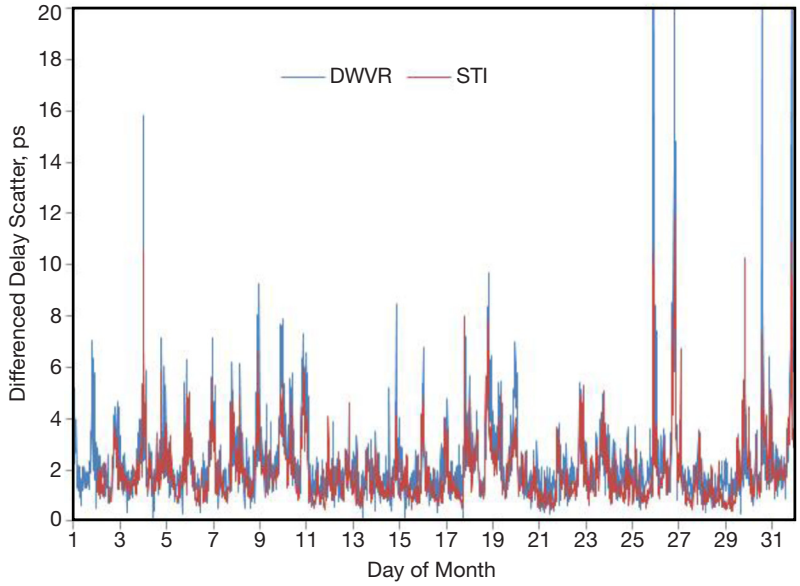

Figure 9. Goldstone Venus STI and DWVR zenith differenced path delay scatter (standard deviation in 1200-s blocks) for August 2008 (thermal noise estimates removed).

Shown in Figure 10 is an expanded scale plot for a selected period of the August 2008 path delay scatter data taken from Figure 9 to allow for a finer detailed examination of the two data sets. As one can see, the STI path delay fluctuations are closely tracked by the DWVR path delay fluctuations, with some differences including the added noise on the DWVR data set. Thus, we have reasonably good agreement between the path delay scatters measured from two independent instruments within the noise limitations of the suboptimal and aging WVRs that were available and used for this experiment. The DWVR data set thus provides a validation of the STI fluctuations as indeed being atmospheric in nature for this particular case of a warm-weather summer month. It was found that the use of 600-s blocks resulted in a several complications as there was increased noise on the DWVR scatter time series. Thus, the use of 1200-s sized blocks resulted in a much cleaner correlation between the two data types.

By interpolating the STI data to the time tags of the DWVR time series (using the spline method) and performing a difference between data sets, the scatter of the resulting difference was measurably reduced below that of either of the individual data sets. We chose to examine the interval between August 5 and August 25 of the data shown in Figure 9. The resulting differenced residuals are shown in Figure 11. The standard deviation of the STI data that lie within this interval is 1.06 ps, and for the DWVR data the standard deviation is 1.29 ps. The standard deviation of the differenced data is 0.89 ps. Although this improvement is not overly striking, the resulting improvement is encouraging given the deficiencies of the aging WVRs, the nonoptimum data acquisition scheme (WVR time tags not synchronized and calibrations done at different times), and the fact that the STI sample times do not lie exactly on top of the DWVR time tags. Figure 12 displays a segment of the data from Figure 11 on an expanded scale, showing detail of some of the variations. Some of the larger systematic trends such as near days 16.0, 17.0, 17.8, 18.8, and 20.0 appear to repeat with an almost daily periodicity with each peak occurring shortly after local noon. These

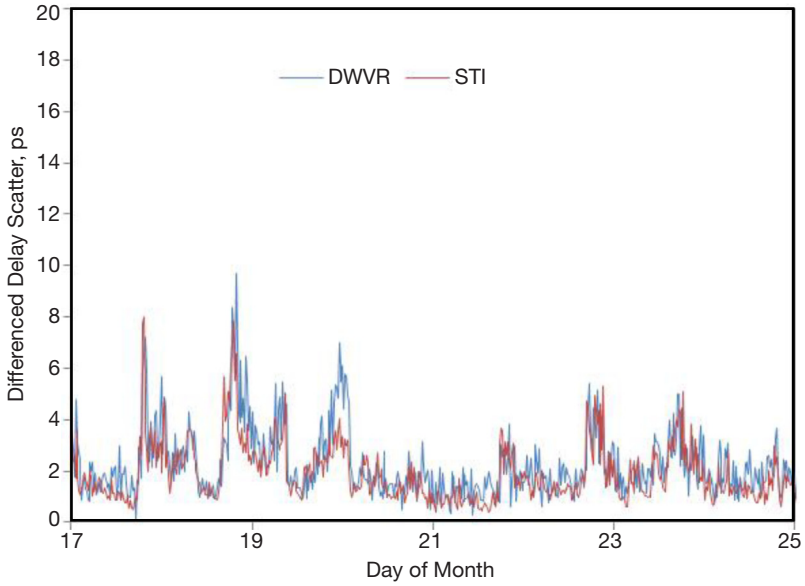

Figure 10. Expanded view of STI and DWVR zenith differenced path delay standard deviation (in 1200-s blocks) time series for the selected several-day period of August 17–25, 2008.

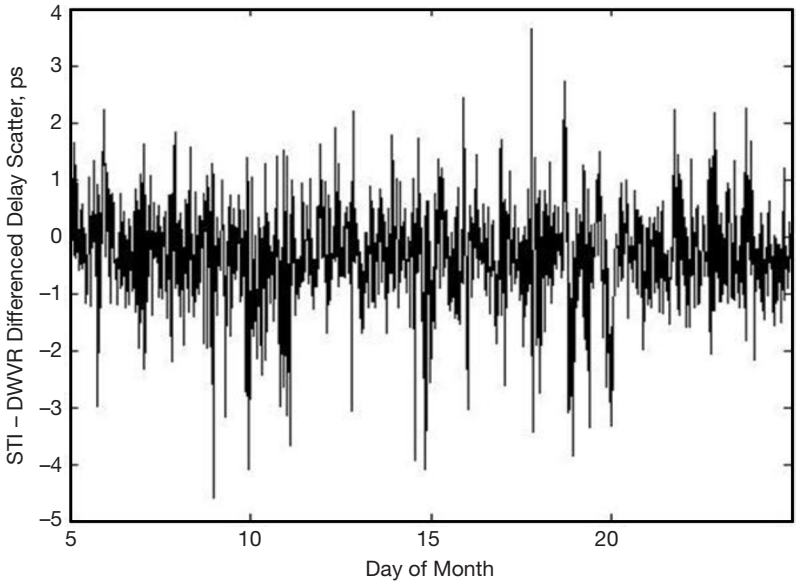

Figure 11. Double difference of STI minus DWVR data interpolated to time tags of DWVR data set.

features may be indicative of equipment deficiencies (during warm humid conditions) that have been discussed elsewhere in this article. Proposed future studies using improved WVRs and optimum data acquisition algorithms are expected to result in measurable improvement and allow for further reduction of nontropospheric contributions in such comparisons. A low-cost, off-the-shelf WVR that possibly can be used for such studies is described elsewhere in this issue [10].

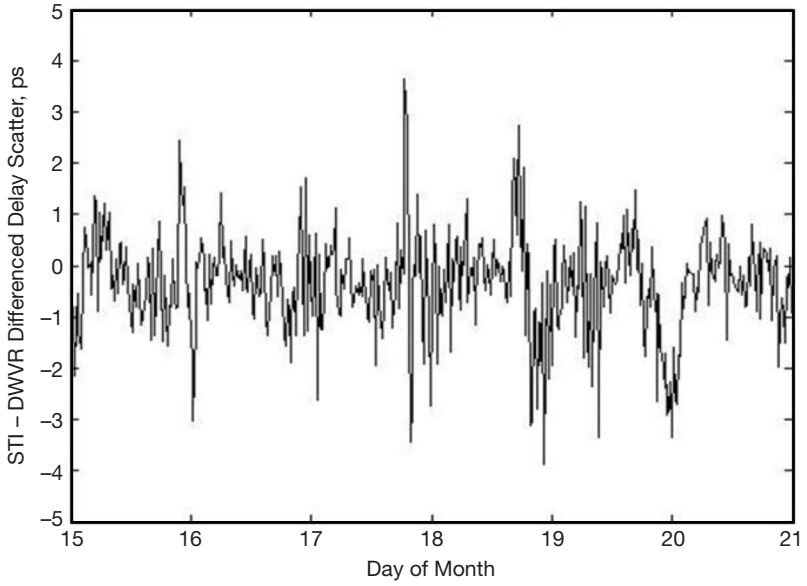

Figure 12. A subset of the double difference data of Figure 11 on an expanded scale showing additional detail.

We also generated cumulative distribution curves of the zenith path delay scatter statistics for the month of August 2008 after quadratically removing estimates of system noise from both data sets (1.3 ps for the DWVR and 0.158 ps for the STI). A few anomalously high valued points from the DWVR data set were removed from the estimation of the CDF. Several of these points did coincide with the few instances of "jumps" in the DWVR differenced data set due to D-unit issues. Figure 13 displays the cumulative distribution function (CDF) of the differenced path delay scatter data for the STI over 1200-s (solid red curve), and, for reference, over 600-s blocks (dotted red curve). As expected, the 1200-s STI curve lies slightly to the left of the 600-s STI curve due to reduced scatter for the longer block period case. Also plotted in Figure 12 is the noisier DWVR CDF over 1200-s blocks lying to the right of the STI curves, and the DWVR 1200-s curve after scaling to the baseline distance of the STI using the 0.95 factor derived from Equation (4). The scaled DWVR CDF curve lies closer to the STI 1200-s CDF curve. A factor of 0.89 (multiplied to the DWVR scatter estimates) provides a better match of the DWVR and STI CDFs. This implies a 5 percent difference due to other effects. Such possible additional error sources are discussed in Section IV. The nature of the various contributions that go into this correction factor is not understood but may include a combination of noise sources such as beam mismatch, additional energy imposed by the interpolation algorithm across characteristic tropospheric timescales (including WVR tipping curve calibration gaps), possible cloud liquid effects, and other (unknown) phenomena.

IV. Discussion of Error Sources and Contributors to Fluctuation Measurements

The STI directly measures the difference in signal delay from a point well above the atmosphere to two antennas, whereas the WVRs measure the thermal emission from the atmosphere at frequencies near a water vapor resonance. From those measurements, the WVRs attempt to "infer" the column density of water vapor along the pointing direction, and from this we can calculate the path delay due to that water vapor. Even if the inference

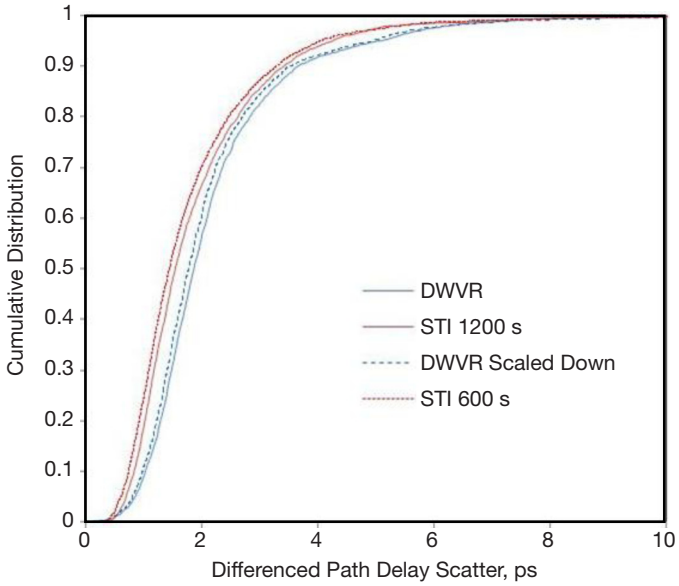

Figure 13. Cumulative distribution of STI zenith differenced path delay scatter in 1200-s blocks (red solid curve), STI path delay scatter in 600-s blocks (red dotted curve), DWVR differenced path delay scatter in 1200-s blocks (blue curve), and DWVR after adjustment of baseline length to that of STI (blue dashed curve).

were perfect, water vapor is not the only cause of path delay. We also have effects from the dry air and from the ionosphere; these are seen by the STI but not by the WVRs. It can be argued that water vapor dominates the fluctuations, and that may be true during the hot summer months, but not always.

Other possible explanations for the differences between the statistics/CDFs for the co-aligned DWVR and STI instrument include interpolation noise, off-point data, beam mismatch, and cloud liquid. Non-water-vapor delay fluctuations may be larger than some of the small effects considered in the article, such as "beam mismatch." We discuss some of these in detail, although additional work is required in order to perform a more thorough comparison of the WVR and STI error budgets in order to assess what type of system and data acquisition scheme would best perform in a particular climate along with cost considerations.

A. Interpolation Error

Interpolation noise is expected to be one contributor of the DWVR error sources in this comparison. However, it is believed that the best approach is to refurbish the WVR units and set them up to sample and integrate at common time tags with equal time durations as well as synchronizing calibrations to minimize gaps. Other improvements that can be realized include having the units operate at much lower system noise temperatures for better sensitivity and thus allow for finer temporal sampling resolution.

We suspect that for the August 2008 data comparison, the contribution of this noise source is comparable to the WVR instrument noise estimate that is magnified during the interpolation process (when using 600-s block sizes). This would be especially larger when interpolating across WVR calibration gaps, as was the case for the present study. Thus, the

interpolation process at different time tags and across calibration gaps is picking up additional energy beyond what would be measured if both WVRs had identical integration and sampling times and synchronized calibrations. The resulting level of several ps in the DWVR path delay above and below that of the STI time series is consistent with this when block sizes of 600 s were studied. By going to larger 1200-s block sizes for the comparison of statistics between the STI and DWVR, the variation in DWVR scatter was reduced and was found to be more agreeable with that of the STI (once the DWVR data were adjusted via removal of the 1.3 ps thermal noise "correction").

Once a suitable DWVR instrument with the above mentioned improvements becomes available and deployed next to an STI, a focus of further study would be to carefully inspect the individual WVR path delay time series prior to differencing and statistical extraction.

B. Data Gaps

Off-point data acquired during WVR tipping curve calibrations (when the WVR beams were not co-aligned with the STI beams) define the gaps addressed by the interpolation scheme and would also contribute to higher scatter. Evaluating this is a focus of further study, but can be minimized using the proposed refined system described above.

C. Beam Mismatch

One component of beam mismatch occurs when the WVR senses a conical volume of sky that is different than that of the STI antenna. The second component is a beam offset error, which is due to the fact that each WVR is not aligned on the axis of its neighbor STI element, but instead is located a few meters away. Theoretical estimates of these errors were computed for the case of a WVR and 34-m-diameter antenna [11–12]. Based on a previous study [11], it was found that at a 10-deg elevation angle, the instantaneous beam mismatch error in path delay was ~1 mm for a 6-deg beamwidth and 0.09 mm for a 0.5-deg beamwidth. It was found that these errors could be reduced by a factor of ~2 or so by higher time averaging. A 50-m offset would result in a modest delay error of less than 0.3 mm for 60-s integration times above a 6-deg elevation angle. The study in [11] assumed conical beams for WVRs and a pencil beam for the 34-m-diameter antenna.

For the current study, we assume the STI antennas have a 1.2-m diameter, a satellite beacon frequency of 20.2 GHz, and a beamwidth of about 6 deg in extent for the WVRs over the brightness temperature frequencies. We can thus make use of the results of [11] discussed in the previous paragraph. At the 48-deg elevation angle of the STI/DWVR combination for this study, this contribution to path delay scatter is believed to lie below that of the WVR/34-m combination estimate of 0.12 mm (0.4 ps) for both WVRs.

An independent limited study assessed this beam mismatch contribution for the 1.2-m STI antenna diameter and the 6-deg WVR beam and found that the resulting error should be ~0.5 mm (or 1.67 ps)[4] assuming 600-s blocks. By assuming 1200-s data blocks, this scatter

[4] Gabor Lanyi, personal communication, Tracking Systems and Applications Section, January 13, 2010.

"ceiling" is reduced to about 0.83 ps. This is comparable to the 0.9 ps scatter of the double difference of the STI and DWVR data sets (see Section III) and below that of the instrumental thermal scatter of 1.3 ps estimated for the floor of the uncorrected DWVR scatter. Thus beam mismatch is one viable contributor to the difference between DWVR and STI statistics.

D. Baseline Length Differences

The correction due to different baseline lengths was addressed at the end of Section II (Equation [4]), and thus it is believed that there is negligible error due to this after this correction is applied.

E. Correlation with Cloud Liquid

One possible contributor of errors in this comparison is cloud liquid (CL), which could skew the results. One expects decidedly better performance from the WVRs during clear conditions. Data taken during cloudy conditions are inherently less accurate and much more subject to lateral variability. In an attempt to evaluate this, we examined the time series of CL estimated from the WVR retrievals.

CL was estimated from linear combinations of the WVR sky brightness temperature data using the appropriate algorithms. For the JT2 unit:

$$L_z = 11.0 - 21.54(\mathrm{TB}_{\mathrm{zen},20.7} - 21.09) + 7.77(\mathrm{TB}_{\mathrm{zen},22.2} - 32.08) + 21.80(\mathrm{TB}_{\mathrm{zen},31.4} - 15.06) \quad (5)$$

where L_z is CL content in microns (μm) referred to zenith and $\mathrm{TB}_{\mathrm{zen,f}}$ is the brightness temperature (K) referenced to zenith at the subscripted sky frequency f (GHz).

Thus, we should be able to indicate clear vs. cloudy periods by correlating the data of Figure 9 repeated in Figure 14(a) with these estimates of CL in Figure 14(b). For this comparison, we only plotted the CL estimates from the J-unit using Equation (5). The estimates from the D-unit were in good agreement and are not plotted here. CL (L_z) values of less than 40 μm (including negative values) are regarded as indicating clear conditions. Values from 40 to 300 μm indicate moderate cloud conditions, or cloud formation in its beginning stages. Values ranging from 300 to 500 μm are indicative of heavy clouds. Values exceeding 500 μm are suggestive of rainy conditions. From Figure 14(b), it appears that August 2008 CL rarely spikes above 300 μm, and thus excessive CL only occurs during a very small fraction of the month. Removing these points from the cumulative distribution analysis does not significantly alter the overall results, and thus we can conclude that the effect of CL on these results is negligible.

V. Future DWVR Experiments and Instruments

A DWVR instrument (co-located with STI) can be used to (1) validate STI statistical results as being tropospheric in nature, (2) help identify problematic co-located STI data periods,

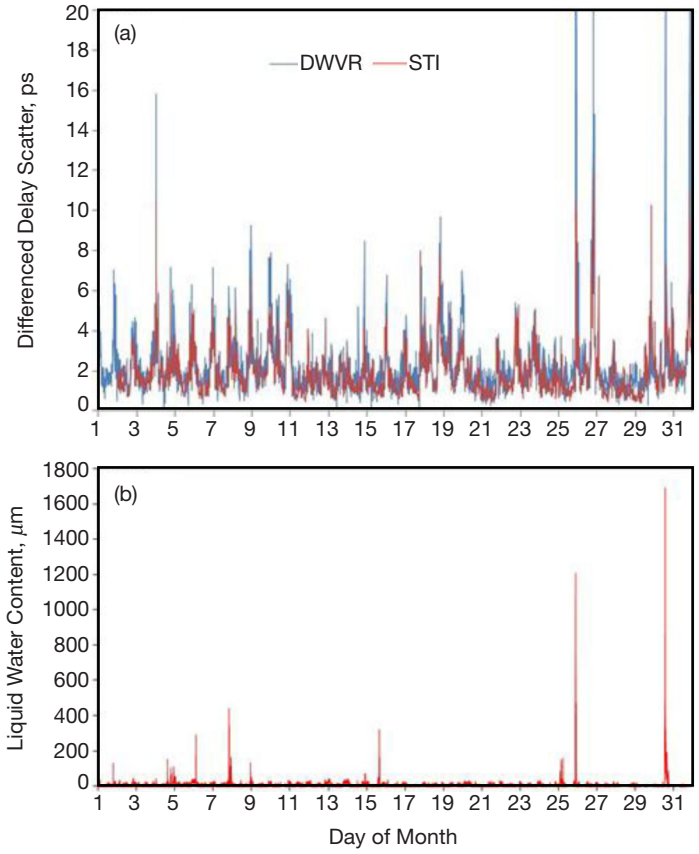

Figure 14. (a) Path delay scatter for STI and DWVR during August 2008 (from Figure 9), and (b) Cloud liquid content extracted from J-unit for August 2008.

(3) potentially be used in place of an STI to acquire atmospheric path delay statistics over ~250-m scales and can be pointed at zenith to facilitate measurements for dry climate sites, (4) could supplement STI data during periods STI is down, and (5) when placed next to elements of an uplink array, could be used to correlate or calibrate atmospheric phase fluctuations from the array observables. Thus, these instruments can be used at array sites to provide estimates of path delay corrections during uplink array activities as well as during downlink array activities such as during periods of weak received signal conditions. DWVRs can be used in place of an STI to assess site suitability for future array configurations when the sites are predominately clear-weather sites and periods of significant moisture are short in comparison to the full-year period. Tracking sites located near polar cap regions would benefit from the use of such an instrument where pointing at geostationary satellite signal sources is not practical and the climates are usually dry due to cold temperatures.

A single-unit WVR along with ancillary meteorological data (wind speed and direction, etc.) could be used to extract similar statistics converting temporal variability to spatial variability to assess site usefulness. In such cases, temporal variability information would be used to infer spatial variability by making use of wind speed and direction data.

The implementation of two high-quality WVRs to perform such experiments would need to be examined in comparison to the quality and cost of deploying an STI. An improved DWVR would require high-quality hardware with identical apertures/equipment and improved algorithms using synchronized calibration sequences, integration intervals, and sample times to allow direct differencing of retrieved path delays. During nominal operation, these instruments could be pointed at zenith to reduce outage or degradation due to rain/cloud saturation, avoid Sun-in-beam issues, etc. (and thus no geostationary satellite source would be required).

A focus of future study would be to evaluate the feasibility of using a DWVR instrument that can be deployed out in the field to generate statistics in place of an STI or complementary to an STI. Available candidate off-the-shelf instruments such as described in [10] can be evaluated for such purposes. In the absence of a coherently generated signal beyond the atmosphere, the DWVR relies on sky brightness temperature, and thus the estimates would be useful when cloud liquid is minimal; thus, statistics would be meaningful during dry periods. Data acquired during wet periods would require special handling techniques. The period of time that liquid content exceeds a threshold using such instruments could serve as a useful statistic in itself. The cloud liquid estimates generated by the WVRs would be useful in defining the percentage of time rainy/cloudy conditions dominate, thus supplementing the dry condition statistics.

VI. Conclusion

An STI was deployed at the Venus (DSS-13) antenna site in Goldstone, California, to assess the suitability of Goldstone as an uplink array site, and statistically characterize atmospheric induced phase fluctuations over a ~250-m baseline for use in future array link scenarios. Beginning in August 2008, two WVR units (DWVR) were deployed next to each Goldstone STI element in an attempt to provide ancillary data that can be used in an intercomparison with the STI phase fluctuations. The results of the inter-comparison presented in this article were encouraging despite the fact that the DWVR data had higher noise contributions. Such an instrument has the potential to make similar-quality measurements in place of or complementary to an STI. By deploying a DWVR instrument of a higher-quality design (lower system noise) using improved algorithms (synchronized sampling and calibrations), improved agreement is expected between STI and DWVR data sets in future intercomparisons.

Acknowledgments

We would like to thank Faramaz Davarian for support of this work, Richard Denning for providing refurbishment support on the WVRs, and Roberto Acosta and James Nestle of NASA GRC for their role in providing the STI data acquired at the Venus Goldstone site.

References

[1] B. Bertotti, L. Iess, and P. Tortora, "A Test of General Relativity Using Radio Links with the Cassini Spacecraft," *Nature*, vol. 425, no. 6956, pp. 374–376, September 25, 2003.

[2] R. P. Linfield, L. P. Teitelbaum, L. J. Skjerve, S. J. Keihm, S. J. Walter, M. J. Mahoney, and R. N. Treuhaft, "A Test of Water Vapor Radiometer–Based Troposphere Calibration Using VLBI Observations on a 21-Kilometer Baseline," *The Telecommunications and Data Acquisition Progress Report*, vol. 42-122, Jet Propulsion Laboratory, Pasadena, California, pp. 12–31, April–June 1995, article dated August 15, 1995. http://ipnpr.jpl.nasa.gov/progress_report/42-122/122I.pdf

[3] G. Elgered, "Tropospheric Radio Path Delay From Ground-Based Microwave Radiometry," Chapter 5, *Atmospheric Remote Sensing by Microwave Radiometry*, edited by M. Janssen, New York: Wiley & Sons, 1993.

[4] L. R. D'Addario, "Combining Loss of a Transmitting Array due to Phase Errors," *The Interplanetary Network Progess Report*, vol. 42-175, Jet Propulsion Laboratory, Pasadena, California, pp. 1–7, November 15, 2008. http://ipnpr.jpl.nasa.gov/progress_report/42-175/175G.pdf

[5] D. D. Morabito and L. D'Addario, "Two-Element Uplink Array Loss Statistics Derived from Site Test Interferometer Phase Data for the Goldstone Climate: Initial Study Results," *The Interplanetary Network Progess Report*, vol. 42-186, Jet Propulsion Laboratory, Pasadena, California, pp. 1–20, August 15, 2011. http://ipnpr.jpl.nasa.gov/progress_report/42-186/186B.pdf

[6] D. D. Morabito, L. D'Addario, S. Shambayati, R. J. Acosta, and J. A. Nessel, "Goldstone Site Test Interferometer Atmospheric Decorrelation Statistics Use in Spacecraft Link Budgets: First Year of STI Data," *Proceedings of the 14th Ka and Broadband Communications Conference*, Matera, Italy, September 24–26, 2008.

[7] R. J. Acosta, J. A. Nessel, and D. D. Morabito, "Data Processing for Atmospheric Phase Interferometers," *Proceedings of the 14th Ka and Broadband Communications Conference*, Matera, Italy, September 24–26, 2008.

[8] J. A. Nessel, R. J. Acosta, and D. D. Morabito, "Phase Fluctuations at Goldstone Derived from One-Year Site testing Interferometer Data,"*Proceedings of the 14th Ka and Broadband Communications Conference*, Matera, Italy, September 24–26, 2008.

[9] G. M. Resch, "Inversion Algorithms for Water Vapor Radiometers Operating at 20.7 and 31.4 GHz," *The Telecommunications and Data Acquisition Progress Report*, vol. 42-76, Jet Propulsion Laboratory, Pasadena, California, pp. 12–26, October–December 1983. http://ipnpr.jpl.nasa.gov/progress_report/42-76/76B.PDF

[10] M. Britcliffe, D. Hoppe and M. Franco, "A Low-Cost Water Vapor Radiometer for Deep Space Network Media Calibration," *The Interplanetary Network Progress Report*, vol. 42-188, Jet Propulsion Laboratory, Pasadena, California, pp. 1–13, February 15, 2012. http://ipnpr.jpl.nasa.gov/progress_report/42-188/188C.pdf

[11] R. P. Linfield and J. Z. Wilcox, "Radio Metric Errors Due to Mismatch and Offset Between a DSN Antenna Beam and the Beam of a Troposphere Calibration Instrument," *The Telecommunications and Data Acquisition Progress Report*, vol. 42-114, Jet Propulsion Laboratory, Pasadena, California, pp. 1–13, August 15, 1993. http://ipnpr.jpl.nasa.gov/progress_report/42-114/114A.pdf

[12] J. Z. Wilcox, "The Effect of Tropospheric Fluctuations on the Accuracy of Water Vapor Radiometry," *The Telecommunications and Data Acquisition Progress Report*, vol. 42-110, Jet Propulsion Laboratory, Pasadena, California, pp. 33–51, August 15, 1992. http://ipnpr.jpl.nasa.gov/progress_report/42-110/110C.PDF